

# Modeling Soot Derived from Pulverized Coal

Alexander L. Brown

Department of Mechanical Engineering, Brigham Young University, Provo, Utah 84602

Thomas H. Fletcher\*

Department of Chemical Engineering, 350 CB, Brigham Young University, Provo, Utah 84602

Received December 10, 1997

A semiempirical model has been developed for predicting coal-derived soot. The main feature of the model is a transport equation for soot mass fraction. Tar prediction options include either an empirical or a transport equation approach, which directly impacts the source term for soot formation. Also, the number of soot particles per unit mass of gas may be calculated using either a transport equation or an assumed average. Kinetics are based on Arrhenius rates taken from published measurements. Radiative properties are calculated as a function of averaged optical constants, predicted gas temperatures, predicted gas densities, and the soot mass fractions. This model has been incorporated into a comprehensive coal modeling code and evaluated based on comparisons with soot, temperature, and NO<sub>x</sub> measurements for three experimental cases. Accurate predictions of soot yields have been achieved for both laminar and turbulent coal flames. Larger scale turbulent predictions illustrated that inclusion of a soot model changed the local gas temperatures by as much as 300 K and the local NO<sub>x</sub> concentration by as much as 250 ppm. These predictions demonstrate the necessity for an accurate soot model in coal combustion systems.

## Introduction

Soot is understood to form in many hydrocarbon flames principally from the combination and condensation of acetylene, benzene, or other aromatic hydrocarbons.<sup>1</sup> At high temperatures in many flames, radiation from typical quantities of soot impacts the energy transfer.<sup>2</sup> Neglecting the soot in a theoretically based model may cause several hundred degrees difference in the predicted flame region. This error in temperature can result in significant error in the chemistry predictions, since kinetic predictions are a strong function of temperature. Soot can also be an emissions problem, even in coal-fired systems. Incorporation of an accurate soot model into comprehensive coal combustion codes is therefore desirable as a means to help describe NO<sub>x</sub> emissions, carbon carryover, and fine particle emission.

Very little information regarding soot formation from coal is available in the literature,<sup>3</sup> and therefore it is important to give an overview of soot formation models for simple hydrocarbons. One approach to soot modeling in simple systems is to develop kinetic mechanisms that describe the soot formation processes.<sup>4,5</sup> While large kinetic mechanisms can be quite accurate, these

methods are computationally intensive and beyond the capabilities of most current comprehensive modeling codes. Despite the inability to use large mechanisms in comprehensive codes, such mechanisms still prove useful in explaining experimental measurements in simple systems as well as serving as benchmarks for reduced mechanisms. Unfortunately, no soot formation mechanisms are available for coal tar, due the complexity of the species involved.

Moss et al.<sup>6</sup> developed a relationship for axis-symmetric laminar gaseous diffusion flames using transport equations for the mass fraction, including nucleation, surface growth, and oxidation source terms. Other researchers have recently used variations of this relationship by solving transport equations for soot number density, soot volume fraction and mass fraction of soot.<sup>7–9</sup> The mass fraction of soot is related to the soot volume fraction by the ratio of the average local gas density to the average soot density:

$$f_{v,C} = (\rho_g/\rho_C) Y_C \quad (1)$$

Most of these studies involve the derivation of new

\* Corresponding author.

(1) Haynes, B. S. Soot and Hydrocarbons in Combustion. In *Fossil Fuel Combustion*; Bartok, W., Sarofim, A. F., Eds.; Wiley & Sons: New York, 1991; pp 261–326.

(2) Siegel, R.; Howell, J. R. *Thermal Radiation Heat Transfer*, 3rd ed.; Hemisphere Publishing Corporation: Bristol, PA, 1992.

(3) Fletcher, T. H.; Ma, J.; Rigby, J. R.; Brown, A. L.; Webb, B. W. *Progress in Energy and Combustion Science* **1997**, *23*, 283–301.

(4) Frenklach, M.; Wang, H. *Twenty-Third Symposium (International) on Combustion*; The Combustion Institute: Pittsburgh, PA, 1990; pp 1559–1566.

(5) Leung, K. M.; Lindstedt, P.; Jones, W. P. *Combust. Flame* **1991**, *87*, 289–305.

(6) Moss, J. B.; Stewart, C. D.; Syed, K. J. *Twenty-Second Symposium (International) on Combustion*; The Combustion Institute: Pittsburgh, PA, 1988; pp 413–423.

(7) Kennedy, I. M.; Kollmann, W.; Chen, J. Y. *Combust. Flame* **1990**, *81*, 73–85.

(8) Honnery, D. R.; Kent, J. H. *Twenty-Fourth Symposium (International) on Combustion*; The Combustion Institute: Pittsburgh, PA, 1992; pp 1041–1047.

(9) Sivathanu, Y. R.; Gore, J. P. *Combust. Flame* **1994**, *97*, 161–172.

estimates for the nucleation, surface growth, and oxidation terms. In a study by Coelho and Carvalho,<sup>10</sup> two different soot formation models were coupled with three different oxidation models taken from different researchers in an effort to determine which models best correspond to measured data. These reaction models were coupled with the conservation equations for the number densities and concentrations of soot. Comparisons were made regarding the predictions of soot in a turbulent propane diffusion flame between the various combinations of models and measured data. More evaluations using this general approach have been performed, including modeling of a turbulent three-dimensional flame.<sup>7,11,12</sup> In all of these studies, reasonable agreement existed between measured soot volume fractions and predicted ones.

None of the above-mentioned methods apply to coal-derived soot since tar, rather than acetylene, is the principal precursor to soot in coal flames. Coal devolatilization experiments in inert gas have shown that the mass of soot plus tar remains relatively constant after primary devolatilization.<sup>13–16</sup> Gas products have been quantified for many coals; acetylene and benzene have not been shown to exist in significant quantities.<sup>17</sup>

Three previous attempts at coal soot modeling have been made, all of which rely heavily on empirical assumptions to make the soot predictions. Ubhayaker et al.<sup>18</sup> used an empirical relationship based on the mole fraction of CO to estimate the amount of soot in a coal devolatilization experiment, although no soot data were presented. Adams and Smith<sup>19</sup> assumed that due to oxidation, soot exists where the local equivalence ratio ( $\phi$ ) is 1.0 and above, and increases linearly to a maximum value at an equivalence ratio of 2.0 and above. An empirical function was developed to describe the dependence of soot yield on  $\phi$ :

$$C_2 = \text{Max}(0.0, \text{Min}(\phi - 1.0, 1.0)) \quad (2)$$

The maximum soot volume fraction was calculated as a direct function of the amount of volatile carbon found to exist at that point. It was assumed that 10% of the volatile carbon forms soot ( $C_1 = 0.1$ ). The soot volume fraction was then calculated as follows

$$f_{v,C} = C_1 C_2 \beta_C M_C / \rho_C \quad (3)$$

(10) Coelho, P. J.; Carvalho, M. G. *ASME: Heat Transfer in Fire and Combustion Systems*; ASME: Fairfield, NJ, 1994; p 272.

(11) Fairweather, M.; Jones, W. P.; Lindstedt, R. P. *Combust. Flame* **1992**, *89*, 45–63.

(12) Moss, J. B.; Stewart, C. D.; Young, K. J. *Combust. Flame* **1995**, *101*, 491–500.

(13) Chen, J. Effect of Secondary Reactions on Product Distribution and Nitrogen Evolution from Rapid Coal Pyrolysis. Ph.D. Dissertation (Mechanical Engineering), Stanford University, Palo Alto, CA, 1991.

(14) Ma, J. Soot Formation and Secondary Reactions During Coal Pyrolysis. Ph.D. Dissertation (Chemical Engineering), Brigham Young University, Provo, UT, 1996.

(15) Nenniger, R. D.; Howard, J. B.; Sarofim, A. F. *Proceedings of the 1983 International Conference on Coal Science*; 1983; p 521.

(16) Wornat, M. J.; Sarofim, A. F.; Longwell, J. P. *Energy Fuels* **1987**, *1*, 431.

(17) Smith, K. L.; Smoot, L. D.; Smith, P. J. *The Structure and Reaction Processes of Coal*; Plenum: New York, 1994.

(18) Ubhayaker, S. K.; Stickler, D. B.; von Rosenberg, C. W.; Gannon, R. E. *Sixteenth Symposium (International) on Combustion*; The Combustion Institute: Pittsburgh, PA, 1976; pp 427–436.

(19) Adams, B. R.; Smith, P. J. *Combust. Sci. Technol.* **1995**, *109*, 121–140.

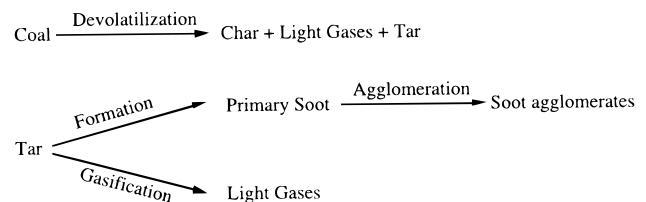


**Figure 1.** Presumed pathways for coal devolatilization and soot formation.

where  $\beta_C$  was the moles of carbon per unit mass in the reactor. It is unclear how the units in this equation were justified (i.e., a gas density is needed in the numerator), which may have led to errors in their method. Adams and Smith concluded that the inclusion of a soot radiation model increased predicted radiative transfer in a pulverized coal flame; however, the maximum local temperature difference between predictions with and without the soot model was lower than expected (only about 50 K). They attributed this result to the soot absorbing nearly as much radiant energy as it emitted. Also, they addressed the need for a more advanced soot model.

Ahluwalia and Im<sup>20</sup> took a similar approach, assuming that 10% of the volatile carbon given off becomes soot. Soot was restricted to the burner zone. Their results indicate that soot is responsible for between 14 and 15% of the total heat transfer in the furnaces modeled.

The objective of this research was to develop an advanced coal soot model that more accurately represents the evolution of the soot. Coal soot is assumed to form from tar, which has a relatively high molecular weight ( $\sim 350$  amu). Tar yields vary with coal type, temperature, heating rate, and pressure. Figure 1 illustrates the assumed pathway for soot formation from coal. To accurately describe coal soot formation, the model should be able to describe both the transport of tar and conversion to soot. Existing coal particle models can describe coal devolatilization based on measured characteristics from the coal.<sup>21–23</sup> These models use various methods of combining statistical, theoretical, and empirical assumptions to predict tar formation. Therefore, in this work, a coal devolatilization model was combined with transport equations (in a manner similar to the techniques used to model gas-derived soot) to model coal soot formation.

## Theoretical Treatment

The approach of Moss et al.<sup>6</sup> and Fairweather et al.<sup>11</sup> may be applied to coal-derived soot by generating the proper conservation equations, source terms, and boundary conditions for three-dimensional calculation of soot mass fraction ( $Y_C$ ), soot particles per unit mass ( $N_C$ ), and tar mass fraction ( $Y_T$ ). In all of these variables, the “per mass”, or fractional mass, represents the total mass of soot particles and gas in a given cell. Initially, an average soot number density was assumed following Kennedy et al.,<sup>7</sup> but preliminary examinations indicated

(20) Ahluwalia, R. K.; Im, K. H. *J. Inst. Energy* **1994**, *67*, 23–29.

(21) Fletcher, T. H.; Kerstein, A. R.; Pugmire, R. J.; Solum, M. S.; Grant, D. M. *Energy Fuels* **1992**, *6*, 414–431.

(22) Niksa, S. A.; Kerstein, R. *Energy Fuels* **1991**, *5*, 647–655.

(23) Solomon, P. R.; Hamblen, D. G.; Carangelo, R. M.; Serio, M. A.; Desphande, G. V. *Energy Fuels* **1988**, *2*, 405–422.

**Table 1. Boundary Conditions for the Transport Equations**

location	soot mass fraction	tar mass fraction	soot particles per unit mass
primary jet	0.0	0.0	0.0
secondary jet	0.0	0.0	0.0
walls	d/dx <sub>⊥</sub> = 0.0	d/dx <sub>⊥</sub> = 0.0	d/dx <sub>⊥</sub> = 0.0
outlet	quadratic	quadratic	quadratic
symmetry plane	extrapolation	extrapolation	extrapolation
	d/dx <sub>⊥</sub> = 0.0	d/dx <sub>⊥</sub> = 0.0	d/dx <sub>⊥</sub> = 0.0

that detailed calculations of the local number density may be important to ensure the accuracy of the model. The boundary conditions for soot mass fraction, tar mass fraction, and the soot particles per unit mass are similar to the boundary conditions for other flowfield variables such as the coal gas mixture fraction ( $\eta$ ) and the mixture fraction variance ( $g$ ), as shown in Table 1.

Axi-symmetric (i.e., 2-D) models in the literature have included an additional thermophoretic velocity in the diffusion term. However, none of the three-dimensional models in the literature employ this term, apparently to simplify numeric calculations; this practice was adopted in the present calculations. The equations for conservation of the mass of soot ( $Y_C$ ) and tar ( $Y_T$ ) are

$$\vec{\nabla} \cdot (\rho_g \vec{u} Y_C) = \vec{\nabla} \cdot \left( \frac{\mu}{\sigma} \vec{\nabla} Y_C \right) + \rho_g S_Y \quad (4)$$

$$\vec{\nabla} \cdot (\rho_g \vec{u} Y_T) = \vec{\nabla} \cdot \left( \frac{\mu}{\sigma} \vec{\nabla} Y_T \right) + \rho_g S_Y \quad (5)$$

assuming that  $f_{v,C}$  is small (i.e.,  $\rho_{tot} \approx \rho_g$ ). The equation for conservation of number of soot particles ( $N_C$ ) is

$$\vec{\nabla} \cdot (\rho_s \vec{u} N_C) = \vec{\nabla} \cdot \left( \frac{\mu}{\sigma} \vec{\nabla} N_C \right) + \rho_g S_N \quad (6)$$

where  $\mu$  is the turbulent viscosity,  $\sigma$  is the turbulent Schmidt number,  $\rho$  is the time-averaged density, and  $u$  is the Favre-averaged velocity. Diffusivity is represented through the turbulent Schmidt number; standard values of the Schmidt number (700) are used for the transport equations for  $Y_C$  and  $N_C$ .<sup>7,11</sup> For the tar mass fraction equation ( $Y_T$ ), 0.7 was assumed for the Schmidt number, which is the value commonly assumed for the gas-phase Schmidt number.<sup>24</sup>  $S$  represents the source terms for each transport equation. Soot and tar source terms were derived based on the assumed pathways illustrated in Figure 1. The source terms for the  $N_C$  equation were derived following Fairweather et al.<sup>11</sup> The  $N_C$  agglomeration term comes from the Smoluchowski particle rate equation, as described by Haynes<sup>1</sup> and Ulrich.<sup>25</sup> The possible contribution from light gases to the formation of soot has been neglected in the formulation of this model. Source terms for eqs 4–6 are listed below:

$$S_{Y_C} = \dot{r}_{FC} - \dot{r}_{OC} \quad (7)$$

$$S_{Y_T} = \dot{r}_{FT} - \dot{r}_{FC} - \dot{r}_{GT} - \dot{r}_{OT} \quad (8)$$

$$S_{N_C} = (N_a/M_C C_{\min}) \dot{r}_{FC} - \dot{r}_{AN} \quad (9)$$

where

$$\dot{r}_{FT} = S P_{\text{tar}} \quad (10)$$

$$\dot{r}_{OT} = \rho_g [c_T] [c_{O_2}] A_{OT} e^{-E_{OT}/RT} \quad (11)$$

$$\dot{r}_{GT} = [c_T] A_{GT} e^{-E_{GT}/RT} \quad (12)$$

$$\dot{r}_{FC} = [c_T] A e_{FC}^{-E_{FC}/RT} \quad (13)$$

$$\dot{r}_{OC} = S A_{v,C} \frac{P_{O_2}}{T^{1/2}} A_{OC} e^{-E_{OC}/RT} \quad (14)$$

$$S A_{v,C} = (6^{2/3} \pi^{1/3} (\rho_g N_C)^{1/3} Y_C^{2/3} \rho_g^{2/3}) / \rho_C^{2/3} \quad (15)$$

$$\dot{r}_{AN} = 2 C_a \left( \frac{6 M_C}{\pi \rho_C} \right)^{1/6} \left( \frac{6 k T}{\rho_C} \right)^{1/2} \left( \frac{\rho_g Y_C}{M_C} \right)^{1/6} (\rho_g N_C)^{11/6} \quad (16)$$

The average carbon soot density was assumed to be 1950 kg/m<sup>3</sup>, and the collision frequency constant ( $C_a$ ) was assumed to be 3. Table 2 gives a description of the Arrhenius constants used.

Tar yields were calculated from the Lagrangian particle phase equations which used the CPD model<sup>21</sup> to determine devolatilization rates and tar yields. When <sup>13</sup>C NMR data were not available as input parameters for the CPD model, a correlation was used<sup>26</sup> to estimate <sup>13</sup>C NMR parameters from the proximate and ultimate analysis. One-step rate constants for coal volatile reactions with oxygen for different coals from Shaw et al.<sup>27</sup> were used. Since one aim of this research is to develop a comprehensive model, and Shaw's data do not cover all of the coals, the rate constants were averaged to obtain the rate reported in Table 2. The error introduced by this assumption is thought to be small, since tar is generally released in a fuel-rich region and therefore rapidly converted to soot before significant tar combustion occurs. This approach also ignores OH as an oxidizer, which may be particularly important for lean flames;<sup>28,29</sup> as accurate models of OH concentrations in turbulent coal flames become available, soot oxidation by OH should be included.

Once the value of  $Y_C$  has been calculated from eq 4, the soot volume fraction ( $f_{v,C}$ ) may be calculated using eq 1. The soot emissivity may then be determined using the following method:<sup>30</sup>

$$\epsilon_c = 1 - (1 + 350 f_{v,C} T L_c)^{-4} \quad (17)$$

The emissivity may be related to the absorption coefficient through Bouguer's Law

(26) Genetti, D. B.; Fletcher, T. H. *ACS Division of Fuel Chemistry* **1997**, *42*, 194–198.

(27) Shaw, D. W.; Zhu, X.; Misra, M. K.; Essenhigh, R. H. *Twenty-Third Symposium (International) on Combustion*; The Combustion Institute: Pittsburgh, PA, 1990; pp 1155–1162.

(28) Puri, R.; Santoro, R. J.; Smyth, K. C. *Combust. Flame* **1994**, *97*, 125–144.

(29) Villasenor, R.; Kennedy, I. M. *Twenty-Fourth Symposium (International) on Combustion*; The Combustion Institute: Pittsburgh, PA, 1992; pp 1023–1030.

(30) Sarofim, A. F.; Hottel, H. C. In *Heat Transfer-1978*; Hemisphere Publishing: Washington, DC, 1978; pp 199–217.

(24) Hill, S. C.; Smoot, L. D. *Energy Fuels* **1993**, *7*, 874–883.

(25) Ulrich, G. D. *Combust. Sci. Technol.* **1971**, *4*, 47–57.

**Table 2. Transport Equation Source Terms**

term	A	E (kJ/g·mol)	source
$k_{FT}$	N/A	N/A	particle phase calcs
$k_{OT}$	$6.77 \times 10^5$ (1/s)	52.3	Shaw et al. <sup>27</sup>
$k_{GT}$	$9.77 \times 10^{10}$ (1/s)	286.9	Ma <sup>35</sup>
$k_{FC}$	$5.02 \times 10^8$ (1/s)	198.9	Ma <sup>35</sup>
$k_{OC}$	$1.09 \times 10^4$ (K <sup>1/2</sup> /s)	164.5	Lee et al. <sup>41</sup>
$k_{AN}$	N/A	N/A	Fairweather et al. <sup>11</sup>

$$\kappa = -(1/L_e) \ln(1 - \epsilon) \quad (18)$$

giving

$$\kappa_C = (4/L_e) \ln(1 + 350 f_{v,C} TL_e) \quad (19)$$

This absorption coefficient is then summed with the calculated absorption coefficient for the radiating gases (i.e., CO<sub>2</sub> and H<sub>2</sub>O) to form a total absorption coefficient. More detailed models are reviewed by Brown,<sup>31</sup> but uncertainty in the optical constants and the combined simplicity and estimated accuracy of this correlation do not warrant a more complex model in this study. The mean beam length ( $L_e$ ) requires the assumption that the gas region of the combustor is a homogeneous isothermal medium and is described by the following equation:

$$L_e = 4V/SA \quad (20)$$

The comprehensive code used (PCGC-3) uses a mixing-limited assumption to predict chemistry in turbulent coal flames (i.e., the tar transport equation is only used for the soot model). Local equilibrium is used in conjunction with an assumed-shape PDF approach for major species. The equilibrium code does not properly characterize the rate-limited behavior of NO<sub>x</sub>, therefore a NO<sub>x</sub> postprocessor is used which predicts nonequilibrium NO<sub>x</sub> based on the converged predictions from the equilibrium-based code.<sup>32,33</sup>

The soot model of Adams and Smith<sup>19</sup> was also coded for comparison purposes. Interestingly, upon comparing the two models,<sup>31</sup> the Adams and Smith model appears to predict high soot yields in regions of high tar yield (predicted by the CPD model). It was therefore postulated that Adams' method could be simply modified to predict a mass fraction of tar rather than a soot volume fraction:

$$Y_T = C_1 C_2 M_C \beta_C \quad (21)$$

This option was therefore coded using  $C_1 = 0.35$  (to compensate for the gas density effect) and  $C_2$  from eq 2 and is presented as an alternative to the more complex transport equation solution. This simplified method for predicting tar yield is referred to as the empirical tar yield method. A simple test indicated that tar yields using this equation were on the order of tar yields from eq 5 used in conjunction with the CPD model. Since the iterative techniques used to solve the transport equations represent a significant part of the total

computational load, empirical models present an attractive alternative if correlations for  $C_1$  and  $C_2$  can be developed to better describe the effects of coal type.

Another alternative considered was to assume an average number density, in a manner similar to that used by Kennedy and co-workers.<sup>7</sup> The average value used for the number density ( $\rho N_C$ ) by Kennedy and co-workers ( $1 \times 10^{16}$  particles/m<sup>3</sup>) was adopted in this research and is based on measurements of Axelbaum et al.<sup>34</sup> from ethylene counterflow diffusion flames.

This model for coal-derived soot (along with alternative approaches) was incorporated into PCGC-3, a comprehensive coal modeling code developed at Brigham Young University (BYU).<sup>24</sup>

## Experiments Used for Evaluation

Because data on soot yields in coal flames are difficult to obtain, validation and tuning of the model are difficult. Three experimental cases were selected to evaluate model performance: (1) measured soot yields in a flat flame burner experiment;<sup>14,35</sup> (2) measurements of gas temperatures and NO<sub>x</sub> concentrations in a practical sized test facility, illustrating the impact of including the soot model on overall model performance; and (3) two-color extinction measurements of the average soot volume fraction across a cross section of a laboratory pulverized coal-fired reactor. Descriptions of the three experiments used to evaluate model performance are given below.

**Flat Flame Burner.** The flat flame burner (FFB) is a laminar flow reactor at BYU. Methane and air pass through a 5 cm × 5 cm honeycomb grid to form small diffusion flamelets. The gases ignite near the burner, forming a uniform, thin flame sheet. Coal particles are injected through a narrow 1.5 mm diameter tube in the center of the burner slightly above the tip of the flame sheet (Figure 2). The coal particles used in the experiment were sieved to maintain sizes between 63 and 75 μm. When the FFB is operated in fuel-rich mode, hot product gases cause the coal to devolatilize without the occurrence of oxidation. A suction probe is placed above the flame, which collects the char and soot. The char and soot are separated aerodynamically using a virtual impactor and cyclone system. Total coal-derived soot yields were measured as a function of the height of the probe above the flame surface.<sup>14,35</sup> These data also included measured temperature profiles at various heights and axial positions, char and soot yields from the coal at various heights, and particle and gas velocity measurements at various locations. This apparatus was modeled with a 25 × 25 × 28 grid using PCGC-3, assuming laminar flow, for Pittsburgh No. 8, Illinois No. 6 and Utah Hiawatha coals at 1800 K.

**Fireside Performance Test Facility.** The ABB/CE fireside performance test facility (FPTF) (Figure 3) is a cylindrical laboratory-scale furnace which was also used to make gas temperature and species concentration

(31) Brown, A. L. Modeling Soot in Pulverized Coal Flames. M.S. Thesis (Mechanical Engineering), Brigham Young University, Provo, UT, 1997.

(32) Boardman, R. D.; Eatough, C. N.; Germane, G. J. *Combust. Sci. Technol.* **1993**, *93*, 193–210.

(33) Hill, S. C.; Smoot, L. D.; Smith, P. J. *Twentieth Symposium (International) on Combustion*; The Combustion Institute: Pittsburgh, PA, 1984; pp 1391–1400.

(34) Axelbaum, R. L.; Flower, W. L.; Law, C. K. *Combust. Sci. Technol.* **1988**, *61*, 51–73.

(35) Ma, J.; Fletcher, T. H.; Webb, B. W. *Twenty-Sixth Symposium (International) on Combustion*; The Combustion Institute: Pittsburgh, PA, 1996; pp 3161–3167.

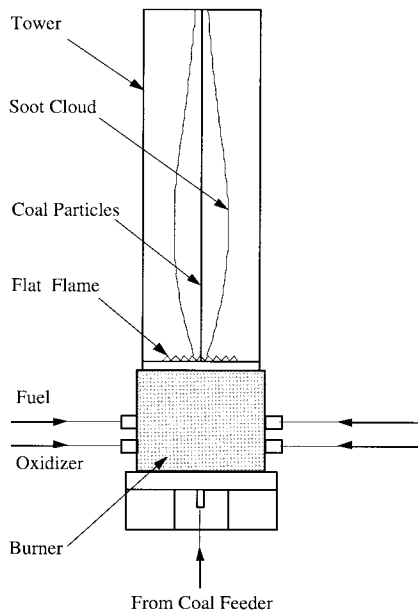


Figure 2. A schematic of the flat flame burner.

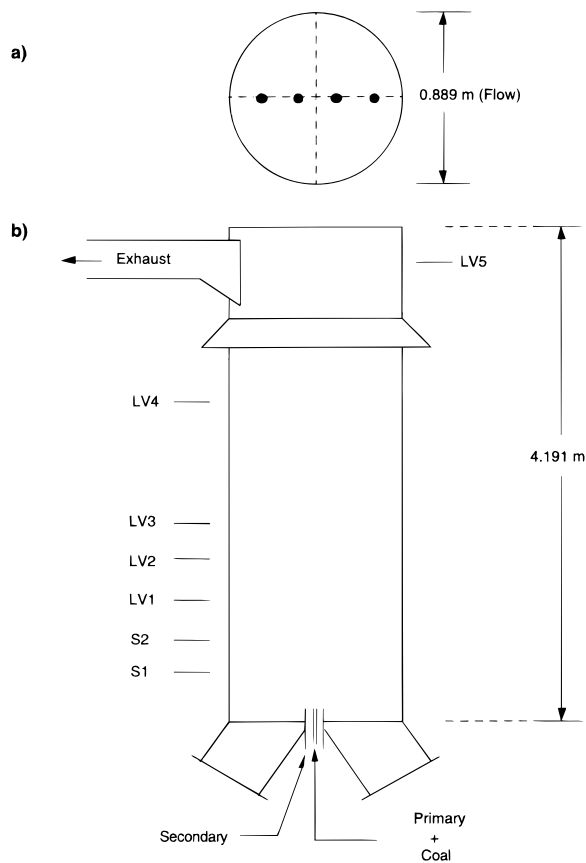


Figure 3. A schematic of the fireside performance test facility.

measurements.<sup>36</sup> The view labeled "a" is a top view, with the major measuring points marked. View "b" is a side view with measurement heights labeled. Test 5, a fuel-lean ( $\phi = 0.83$ ) Ashland (West Virginia) hvA bituminous coal flame, was modeled using a  $69 \times 57 \times 44$  grid. The mass mean particle size was  $41.9 \mu\text{m}$ , the coal feed rate was  $118 \text{ kg/h}$ , the primary air rate was

(36) Thornock, D. E., P. J. Grandia, B. F. Griffith Combustion Modeling: A Combustion Data Set Taken in the Pilot-Scale Fireside Performance Test Facility; ABB Power Plant Laboratories: 1993.

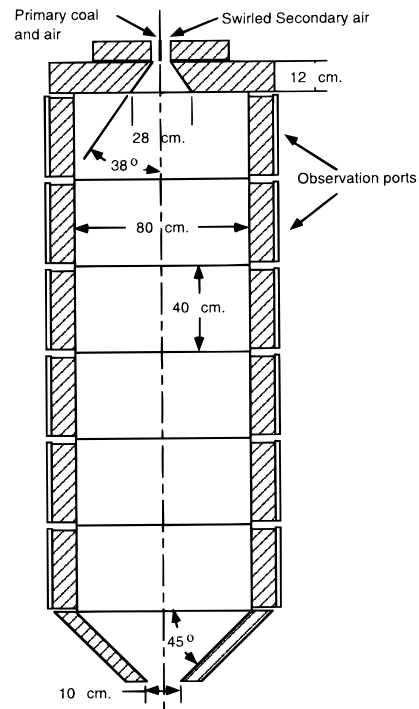


Figure 4. A schematic of the controlled profile reactor.

$100 \text{ kg/h}$ , and the secondary air feed rate was  $1360 \text{ kg/h}$ . The secondary air was modeled with a swirl number of 1.2.

**Controlled Profile Reactor.** The controlled profile reactor (CPR) is a laboratory-scale axi-symmetric pulverized coal-fired furnace that is commonly used to measure detailed radial profiles of gas temperatures and species concentrations for comprehensive model evaluation (Figure 4). Haneberg<sup>37</sup> recently used a two-color extinction technique in this reactor to determine average line-of-sight soot volume fractions at various heights and operating conditions across a centerline cross section. Pickett<sup>38</sup> also measured velocities using laser Doppler velocimetry (LDV) at similar locations and operating conditions. A  $75 \times 75 \times 125$  grid was used to model the furnace at  $\phi = 1.5$  (fuel-rich) and a swirl number of 1.5. The coal used in these experiments was a Wyodak Black Thunder (Wyoming) subbituminous coal.

**Case Nomenclature.** Results for the FPTF and CPR include predictions using various options that have been discussed earlier in this paper. Table 3 gives a description of the nomenclature used to describe the various submodels used in predictions of these two cases. Case 1 represents the best physical description of coal-derived soot. Case 2 does not consider soot at all and is used as a baseline case. Case 3 represents the empirical soot model used by Adams.<sup>39</sup> Case 4 uses an average number of soot particles per unit mass instead of eq 6. Case 5 likewise assumes an average

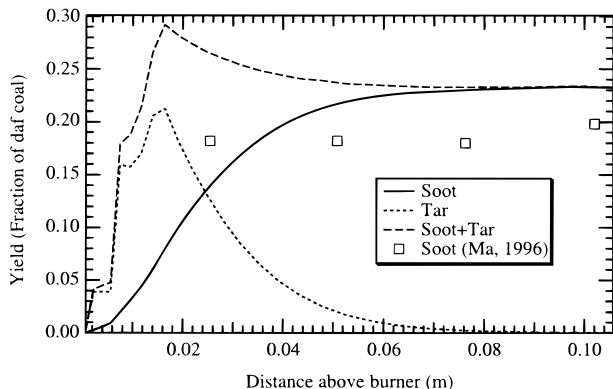
(37) Haneberg, A. L. Soot Volume Fraction Determined by Two-Color Extinction in a Practical Scale Pulverized Coal Flame. M.S. Thesis (Mechanical Engineering), Brigham Young University, Provo, UT, 1997.

(38) Pickett, L. M. Velocity Measurements in a Pulverized Coal Flame Using Laser Doppler Anemometry (LDA). M.S. Thesis (Mechanical Engineering), Brigham Young University, Provo, UT, 1996.

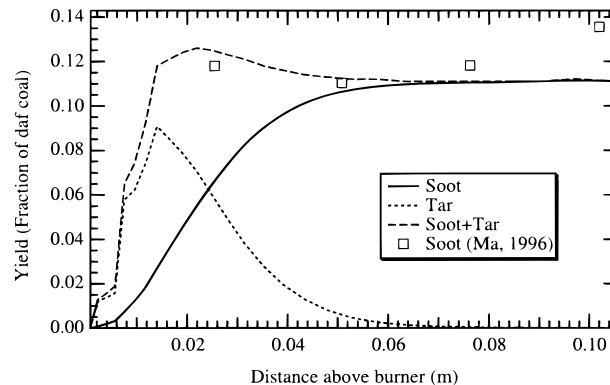
(39) Adams, B. R. Computational Evaluation of Mechanisms Affecting Radiation in Gas-and Coal-Fired Industrial Furnaces. Ph.D. Dissertation (Mechanical Engineering), University of Utah, Salt Lake City, UT, 1993.

Table 3. Description of the Model Test Cases

name	soot	tar	particles per unit mass
Case 1	from transport equation	from transport equation	from transport equation
Case 2	none	none	none
Case 3	from empirical formulation	none	none
Case 4	from transport equation	from transport equation	average assumed
Case 5	from transport equation	from empirical formulation	average assumed
Case 6	from transport equation	from empirical formulation	from transport equation



**Figure 5.** Comparison of predicted and measured soot yields in the FFB for a Pittsburgh No. 8 coal using measured NMR parameters.



**Figure 7.** Comparison of predicted and measured soot yields in the FFB for a Utah Hiawatha coal using the correlation of Genetti et al.<sup>26</sup>

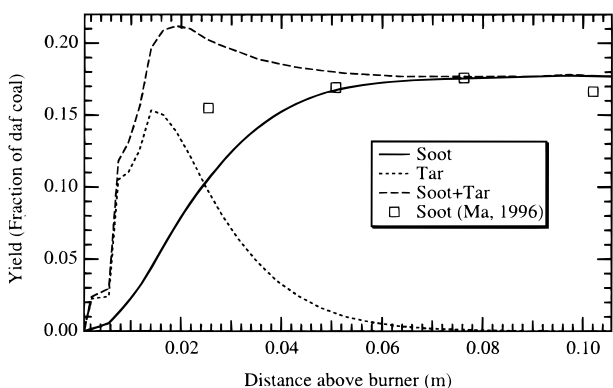


**Figure 6.** Comparison of predicted and measured soot yields in the FFB for an Illinois No. 6 coal using measured NMR parameters.

value of  $N_C$ , and also uses the empirical tar yield assumption for tar formation (eq 21). Case 6, like Case 5, uses the empirical tar yield equation (eq 21) but calculates the number of soot particles per unit mass from the transport equation (eq 6).

## Results

**Flat Flame Burner Predictions.** The flat flame burner provided the best data with which to evaluate the soot formation model. Because  $^{13}\text{C}$  NMR data were not available for the Utah Hiawatha coal, the correlation of Genetti and Fletcher was used to estimate parameters for the devolatilization model.<sup>26</sup> Ultimate soot yields at various heights were predicted quite well for all the coals, as shown in Figures 5–7. Time-dependent predictions were in general agreement with the data, except in the near-burner region. The agreement is not surprising, since the formation model and associated rate coefficients were developed from these data.<sup>14,35</sup> The relatively small amount of disagreement at early residence times is attributed to a combination of uncertainties, including the assumed inlet temperatures, the

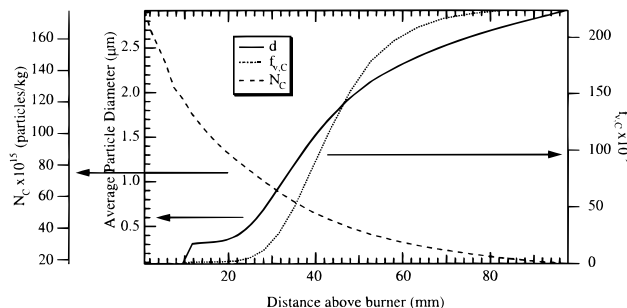


**Figure 8.** Centerline predictions of  $d$ ,  $f_{v,C}$  and  $N_C$  an Illinois No. 6 coal in the FFB.

centerline grid resolution, and the possibility of tars continuing to condense to soot above the quench in the suction probe (measurement locations were taken from the tip of the probe). Ultimately, the soot yields appear to be within or near the bounds of the assumed experimental error of approximately 3% (yield).

The model for soot number density and diameter may also be evaluated based on additional data reported by Ma and co-workers.<sup>35</sup> Between the heights of 25 and 100 mm, the mass of particles with sizes greater than  $5\ \mu\text{m}$  increased from 0 to greater than 50% of the total mass of soot. Corresponding predictions in Figure 8 show a dramatic increase in the number mean diameter of the soot particles along the centerline in this same region. Additionally, these predictions approach  $3\ \mu\text{m}$  at the longest residence times, which may correspond to a mass mean around  $5\ \mu\text{m}$  depending on the size distribution. Figure 8 is representative of the trends in the centerline particle predictions for the other two coals. This comparison lends confidence to the model for soot number density and diameter.

Predicted soot volume fraction contours in the plane through the centerline are shown in Figure 9. Ma et al.<sup>35</sup> reported that the visible soot cloud in this experiment expanded to a diameter of approximately 2.5 cm diameter at the maximum point. The predicted soot

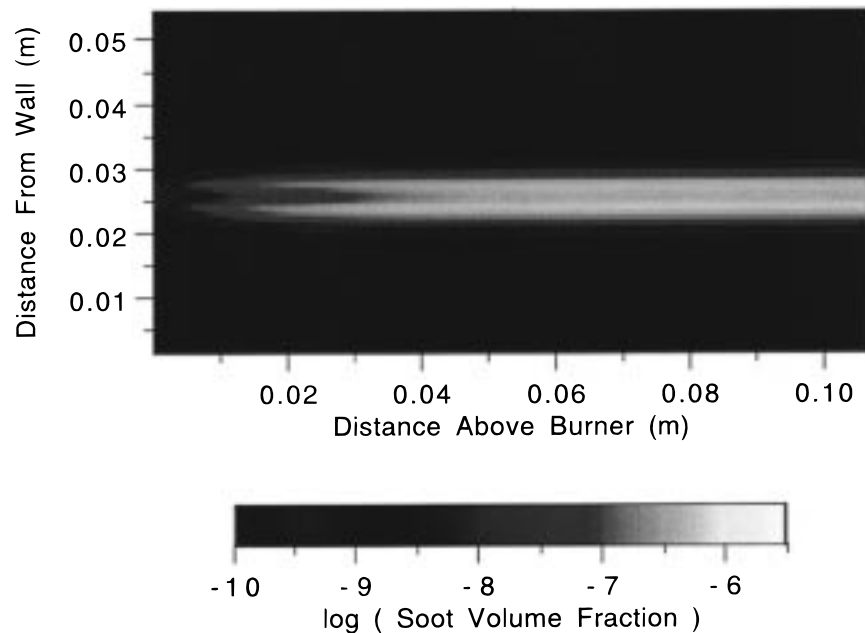


**Figure 9.** Prediction of the soot volume fraction in the FFB for an Illinois No. 6 coal.

cloud diameter is just over half the diameter of the observed luminescent cloud. This is considered reasonable agreement in light of the uncertainty of the observation. However, two effects are omitted which may have reduced the predicted soot dispersion in these laminar-flow predictions: (a) the tar ejection velocity (in the radial direction) from the coal particle; and (b) the thermophoretic diffusivity term in the soot mass fraction equation. These terms are thought to be negligible in practical turbulent systems.

The empirical models for tar and soot (eqs 21 and 3, respectively) were not considered for the FFB because the formation equations rely on the assumption that all carbon in the system is derived strictly from coal. Since methane, CO, and CO<sub>2</sub> are present, soot formation would be over-predicted in this case. This illustrates that the empirical models do not work when additional fuels sources, other than coal (such as natural gas), are used. Gas temperatures and heat transport are not reported for this case because the difference between predictions for Case 1 and Case 2 were found to be negligible due to the small particle loading.

Agreement between the predictions and experimental data in the FFB support many of the assumptions and equations used in generating this model. Although discrepancies exist, particularly in the near burner regions, these problems could be a result of the inability of parts of the combustion code (apart from the soot model) to describe the apparatus. Predicted yields in regions farther above the burner are quite accurate. The limited and qualitative size data support the use of the  $N_C$  variable to predict the expected soot particle diameters. The observed radial dispersion of the visible soot cloud also conforms reasonably well to experimental observations.

**Fireside Performance Test Facility Predictions.** Predictions and measurements of gas temperature and NO<sub>x</sub> concentrations in the FPTF at two different heights are shown in Figures 10–13. Gas temperature and NO<sub>x</sub> profiles near the burner show more spikes than indi-

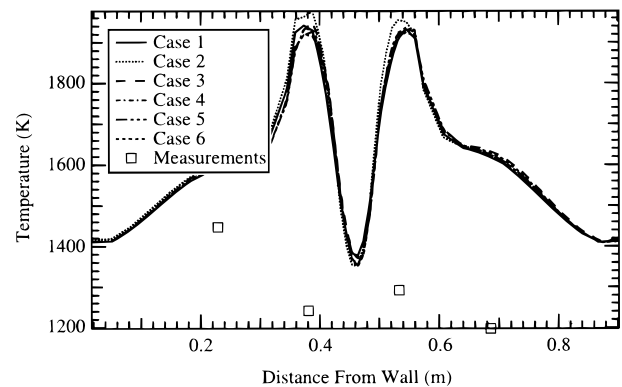


**Figure 10.** Predicted and measured gas temperatures in the FPTF at 68.6 cm above the inlet.

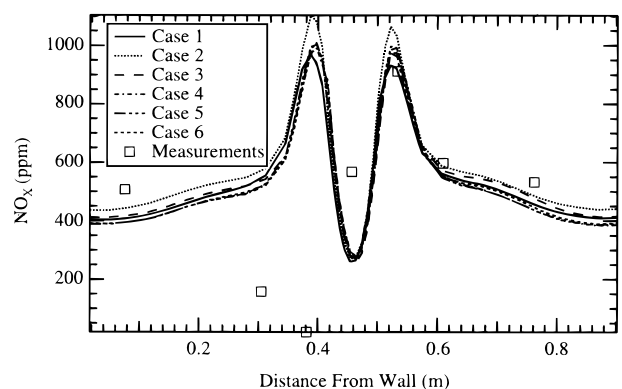


**Figure 11.** Predicted and measured NO<sub>x</sub> concentrations in the FPTF at 68.6 cm above the inlet.

cated by the experimental data, which may be from the use of probes in highly swirling flows. Discrepancies between measurements and predictions existing in the flow field can be attributed to a combination of the inlet grid resolution, the  $k-\epsilon$  turbulence model, and the chemistry model. Predictions for this case seemed to agree well with the experimental measurements at downstream locations. Predictions with and without a treatment of soot were compared to determine the effect

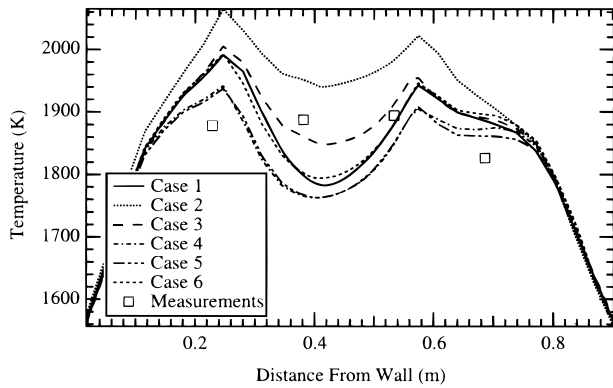


**Figure 12.** Predicted and measured gas temperatures in the FPTF at 144.8 cm above the inlet.

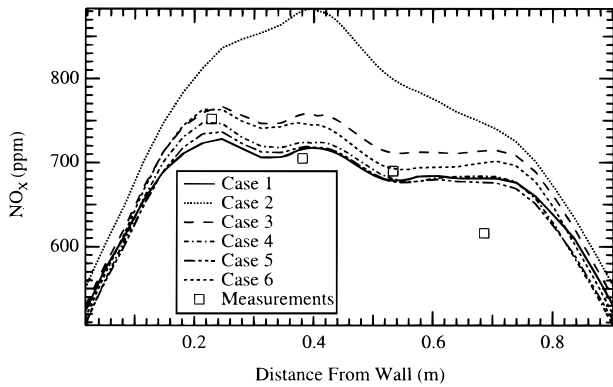


**Figure 13.** Predicted and measured  $\text{NO}_x$  concentrations in the FPTF at 144.8 cm above the inlet.

**Table 4. Maximum Difference between Gas Temperature and  $\text{NO}_x$  Concentration Predictions with and without Soot at Various Heights**

height above the burner (cm)	max gas temp difference (K)	max $\text{NO}_x$ concn difference (ppm)
30.5	54.1	115.4
68.6	92.9	188.0
106.7	109.6	234.2
144.8	183.8	206.9
182.9	281.8	196.9
259.1	138.2	153.3

of treating soot radiation in a coal flame. Table 4 shows the calculated maximum difference between Case 2 and any of the other cases at the heights where experimental data were available. Gas temperature predictions were affected by as much as 300 K and  $\text{NO}_x$  predictions were affected by as much as 250 ppm when soot radiation was ignored. The soot models also predict both the magnitude and trends of the data somewhat better than does the model without considering soot (see Figures 12 and 13).

Cases 1, 3–6 were used to evaluate different aspects of the soot model. Two-dimensional contour plots of  $Y_C$ ,  $Y_T$ , and  $N_C$  better illustrate the differences between the models than the 1-D profiles in Figures 10–13. Figure 14 shows  $Y_T$  predictions using (a) the CPD/transport tar model (case 1) and (b) the empirical tar model (eq 21; Case 6). Predictions appear significantly different depending on the model used both in the maximum concentration and in the spatial distribution. The transport equation method results in higher maximum concentrations in a more compact volume when compared with the empirical method.

A comparison of predictions of  $N_C$  made for (a) Case 1 (CPD/transport tar model) and (b) Case 6 (eq 21; empirical tar model) is shown in Figure 15. Values of  $N_C$  exhibited a tendency to diverge in the region closest to the burner. To maintain the robustness of the model, an upper constraint was placed on the  $N_C$  variable of  $10^{20}$ . This represents the number of incipient-sized soot particles that would occupy half of the volumetric region based on a rough calculation. With the exception of the near-burner region, the values for the  $N_C$  variable vary only slightly within the flame. There is a minor decrease in the predicted values of  $N_C$  progressing downstream from the maximum region of tar, indicating the expected trend toward agglomeration in that region. In regions of low soot mass fraction, the minimum predicted soot particles per unit mass was surprisingly high (compare Figure 14). High values of  $N_C$  in regions of low  $Y_T$  occurred in the FFB and the CPR predictions as well. No data exist in the literature to explain this occurrence. From eq 9, it can be seen that agglomeration is the only pathway considered for soot particle number reduction. The only other pathway that contributes significantly to the reduction of  $N_C$  is oxidation. In the absence of a mechanism for reducing  $N_C$ , values of  $N_C$  in regions of low soot concentrations therefore remain high. Further research is needed in this area to more accurately represent the soot particle count.

Soot volume fraction predictions using the various soot models are shown in Figures 16 and 17. The changes in predictions of  $f_{v,C}$  caused by assuming an average value of  $N_C$  is illustrated by comparing Figure 16a to 16c (using the CPD/transport model) and Figure 17a to 17b (using the empirical tar model). The use of a constant value of  $N_C$  seems to have minimal impact on the prediction of the soot volume fraction for this coal flame. The changes made to predictions of  $f_{v,C}$  due to the use of the empirical tar equation are seen by comparing Figure 16a to 17b (when  $N_C$  transport equation was used) and Figure 16b to 17a (when  $N_C$  was held constant). When the empirical tar equation is used, a slightly lower maximum value for  $f_{v,C}$  is predicted, and the region of maximum soot is predicted to be further away from the burner. However, the similarity in the predicted soot field is surprising, particularly considering the significant differences between the tar predictions illustrated in Figure 14.

Soot volume fraction predictions for the various cases illustrate the impact of the different  $Y_T$  and  $N_C$  models on the  $Y_C$  equation as well as the differences between the empirical predictions of Adams and Smith<sup>39</sup> and the new models. Excluding the  $N_C$  equation (Cases 4 and 5) did not significantly impact the resulting soot volume fraction predictions. This suggests that assuming an average soot number density is not a bad assumption for this case; using the  $N_C$  equation may not be worth the extra computational time required to solve this variable. More testing on additional cases is necessary to determine the extent to which this assumption is valid. Despite the minimal impact on resulting soot predictions, an apparent benefit of using this  $N_C$  equation is the ability to predict average soot particle size. Predictions of soot particle size are important in radiation models, especially if the sizes are large enough to require a treatment of radiation scattering.

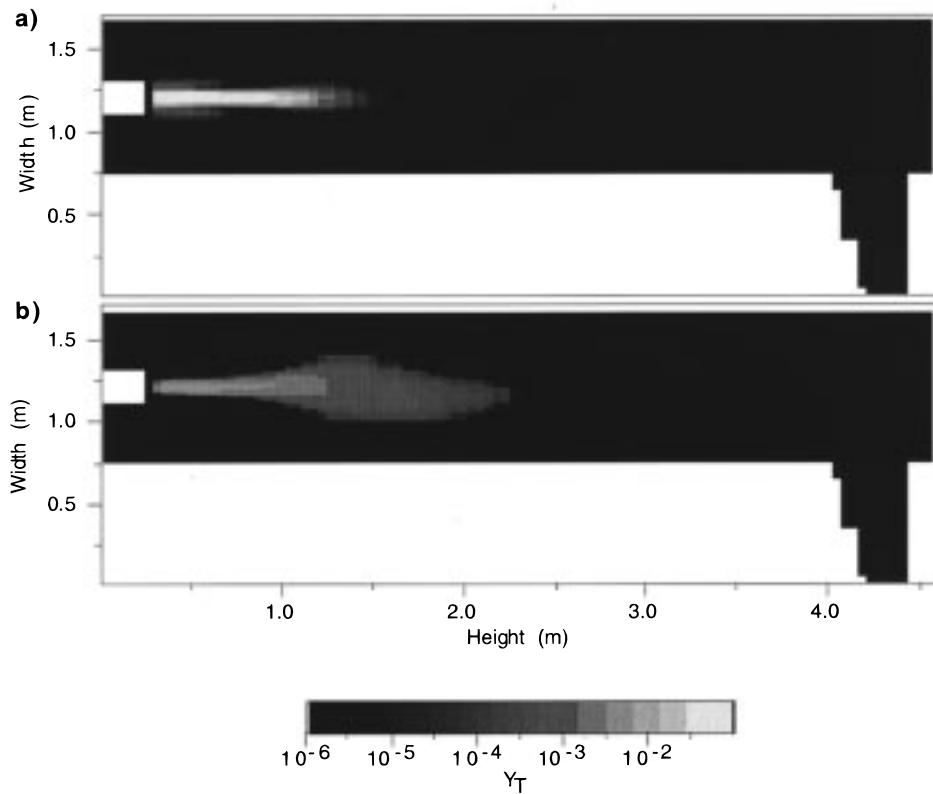


**Figure 14.** Predicted contours of  $Y_T$  in the FPTF. The plot labeled “a” is from Case 1, and the plot labeled “b” is from Case 6.

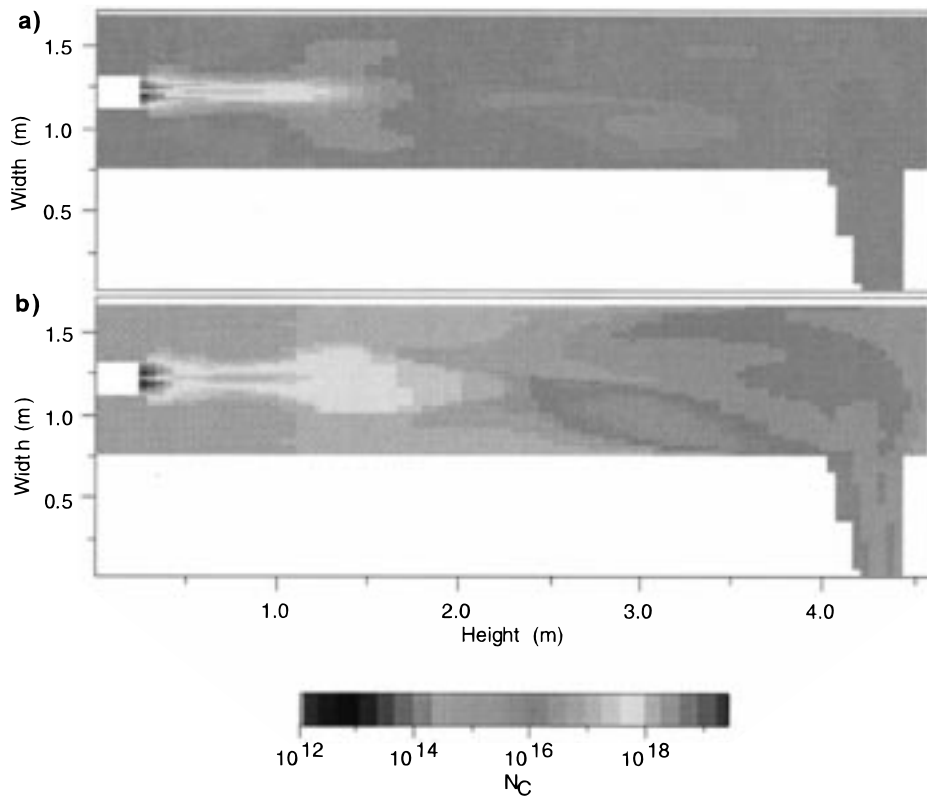


**Figure 15.** Predicted contours of  $N_C$  in the FPTF using the transport equation. The plot labeled “a” is from Case 1, and the plot labeled “b” is from Case 6.

The empirical tar equation predicts significantly lower quantities of tar in the maximum regions, but the tar is spread out over a longer region. Overall, this results in predictions of quantities of soot similar to those of the complete model, and similar soot contours. While the use of the CPD model for tar source term predictions

is likely to result in more accurate tar predictions, results from this model suggest that in the absence of such a model (CPD), the empirical tar formulation may serve as a reasonable approximation. This result is one of the most surprising results from this research, especially since the somewhat arbitrarily assumed  $C_1$

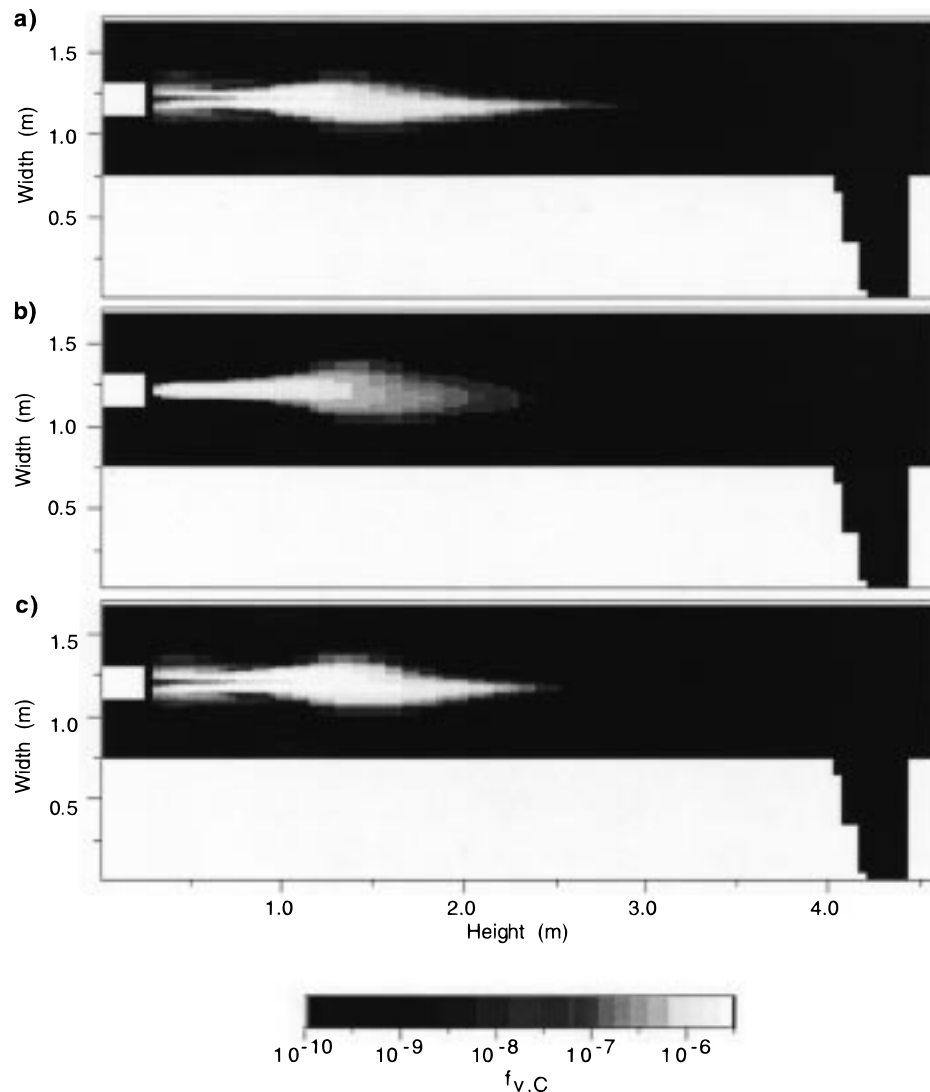


**Figure 16.** Predicted contours of  $f_{v,C}$  in the FPTF. The plot labeled “a” is from Case 1, the plot labeled “b” is from Case 3, and the plot labeled “c” is from Case 4.

variable did not need to be modified from the assumed value for the empirical soot model (at least for the coal in this experiment). Although the equations used to predict the empirical tar formation understandably represent the coal volatiles to a certain extent, the reason that distinct tar predictions would result in such similar soot volume fraction predictions remains without a good theoretical explanation. The good agreement between the CPD/transport tar model and the empirical tar model is likely case-dependent. Further testing, particularly with a broader range of coals, is recommended to determine the extent of the accuracy of this empirical assumption for tar formation.

The good agreement between the data and the numerical predictions as well as the total impact on gas temperatures and  $\text{NO}_x$  concentrations for this case illustrate the necessity for including a model that will accurately predict the soot field and account for the radiative effects.

**Controlled Profile Reactor Predictions.** Modeling the BYU controlled profile reactor has been extremely challenging, especially in three dimensions.<sup>40</sup> The high degree of swirl in this reactor, along with

operating conditions that seem to cause slow fluctuations between partially stable numerical solutions, have made it difficult to perform meaningful detailed radial comparisons of simulations and experiments. Such numerical instabilities may be indicative of physical instabilities in the experiments. In any case, detailed velocity measurements were available for the inlet and flow regions,<sup>38</sup> yet the inlet region still proved too difficult to model accurately.<sup>31,40</sup> However, since the only optical measurements of soot volume fraction for a coal flame were available in this reactor, it was desirable to make at least a semiquantitative comparison with modeling results. Therefore, the range of predicted soot volume fractions from partially converged simulations that best represented the inlet flow conditions and were nearly stable will be shown here.

The optical measurements were performed along a line-of-sight passing horizontally through the reactor centerline, and hence the soot volume fraction deduced from the extinction measurements corresponds to a spatially averaged value.<sup>37</sup> Model predictions of  $f_{v,C}$

(40) Brown, A. L.; Fletcher, T. H. Modeling Soot in Coal Combustion Flames. *Western States Section of the Combustion Institute*; Los Angeles, CA, 1996.

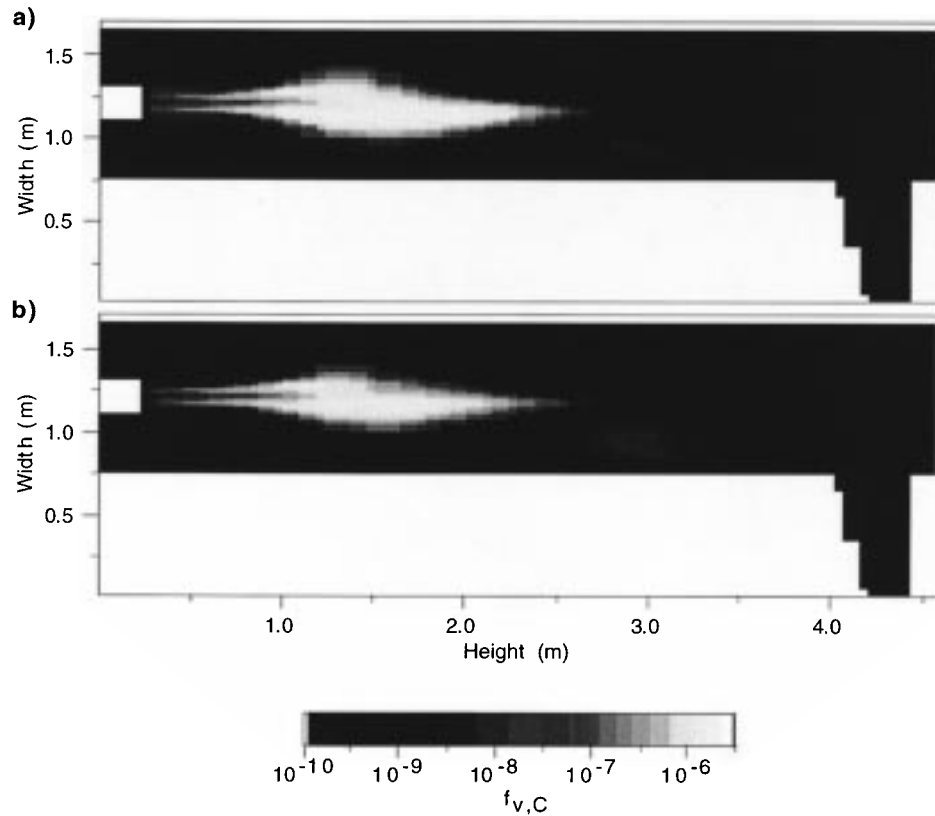


Figure 17. Predicted contours of  $f_{v,C}$  in the FFB. The plot labeled “a” is from Case 5 and the plot labeled “b” is from Case 6.

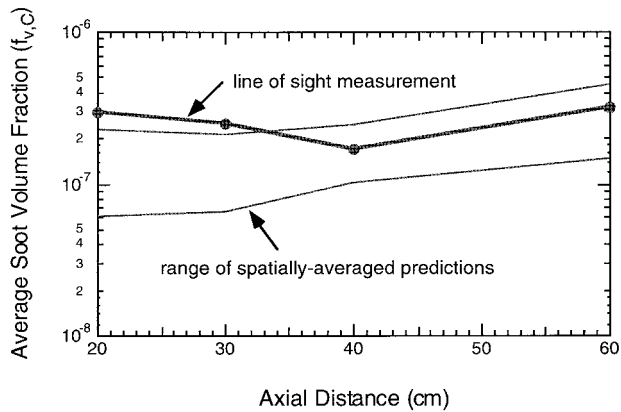


Figure 18. Comparison of line-of-sight measurements of  $f_{v,C}$  with corresponding spatially averaged predictions at various heights in the CPR.

were therefore spatially averaged along the same line of sight as the experiments and are compared with the corresponding measurements as a function of distance from the burner in Figure 18. The range of predicted line-of-sight values shown in Figure 18 are therefore maximum and minimum values of about 10 different nearly-converged solutions. The range of spatially averaged values of  $f_{v,C}$  for this reactor was the same order of magnitude as the optical measurements in this high equivalence ratio case. Model predictions were slightly lower than measurements in regions closer to the burner. In the two regions further away from the burner, the measurements fell within the spread of the predictions. The agreement between the data and the predictions is very encouraging, and should be pursued in a more quantitative and spatially resolved manner.

### Discussion

The proposed soot model, after incorporation into a comprehensive coal combustion model, has been shown to (a) change local predicted gas temperatures in the flame zone by as much as 300 K and (b) change local predicted  $\text{NO}_x$  concentrations by as much as 250 ppm. The laminar flow predictions in the FFB were able to describe the effects of coal type using one set of rate coefficients; only the chemical structure parameters for each coal type were changed, which in turn changed the tar yield during devolatilization. This agreement helps support the proposed formation and oxidation mechanisms for soot and tar and suggests that the soot formation mechanisms from coal tar may be largely independent of coal type. The relative agreement between the predicted soot diameters and the observed diameter information suggests that the equation for  $N_C$  can be used with some confidence. The relative agreement between the predicted radial dispersion of the soot cloud (based on  $f_{v,C}$ ) and the visual observations were also very encouraging, although some additional processes such as radial ejection of tar and thermophoresis may need to be treated in order to improve agreement.

The full soot model significantly impacts the convergence time. To demonstrate the impact of including the soot model, the FFB and FFBTF predictions were timed for a single macroiteration, with and without using the soot model equations. The resulting computational time is illustrated in Table 5. The use of the full soot model increases computational time by 35–48%, due to the inclusion of three new transport equations. Computational time can be reduced by using one or more of the empirical options to start the calculations, followed by

**Table 5. Single Macroiteration Run Times for Two Models**

model	Case 1 (min)	Case 2 (min)
FFB	10.7	6.93
FPTF	317	235

use of the full soot model when flow field calculations are somewhat converged.

A major benefit of the new soot model is that it represents a reduction in empiricism compared to the previous modeling efforts. Reduction in empiricism is likely to result in improved robustness as well as more accurate predictions. The improved robustness of the new model is demonstrated in the fact that the empirical models are incapable of predicting soot in the FFB case. Also, no rational method has yet been developed to determine yield parameters for the empirical soot and/or tar models (i.e., values of  $C_1$  and  $C_2$ ). Because the newly developed method is similar to soot modeling efforts in simpler hydrocarbon flames, the inclusion of a model to account for acetylene, benzene, or soot derived from similar sources would be simply a matter of adding source terms to the existing equations. However, since coal tar is the principal sooting agent in coal flames, the addition of an acetylene-based soot formation mechanism seems unnecessary at this time.

Despite the somewhat limited agreement with the data for oxidizing flames, the model demonstrates the necessity for consideration of soot in comprehensive coal prediction codes. An increase in the amount of predicted soot causes a change in predicted gas temperatures and  $\text{NO}_x$  concentrations. The fact that inclusion of a soot model lowers the predicted local gas temperature in the flame zone by as much as 300 K and  $\text{NO}_x$  concentration by as much as 250 ppm in the FPTF adds credence to the assertion that including a soot model in coal flame predictions is important. Additionally, it appears from the FFB, CPR, and FPTF predictions that the effects of soot increase with the larger sized furnaces. Since the furnaces modeled were smaller test scale models, the effect of accounting for soot may be even more important for the large industrial-scale furnaces. This is certainly true based on qualitative visual observations of coal flames in industrial processes, which visually appear extremely bright.

Predictions from the model for this reactor showed reasonable agreement with the optical measurements in a high equivalence ratio coal flame. The range of model predictions was only slightly lower than measurements in regions close to the burner, but the measurements fell within the spread of the predictions in regions far from the burner. Even though the predictions and measurements were spatially averaged and only semiquantitative, this is the first known comparison of predictions and measurements of soot in a pulverized coal combustion system.

### Recommendations

The lack of reliable soot and tar measurements taken in coal flames hindered model evaluation. Measurements that overcome the inherent interference from coal, char, and ash particles present during the burning of the coal would greatly aid model development and evaluation. Also, the oxidation term for the tar is

questionable, since it was derived from different coals than were used in the predictions presented here and since the rate used was originally developed for simultaneous combustion of both light gas and tar. The predicted tar yield is sensitive to the tar kinetics, and uncertainties in predicted tar yields may detract from the reliability of the soot model. Soot oxidation is a function of the soot particles per unit mass, which has been shown to yield questionable results in regions of low soot. Although the particle count appears to have a minimal effect on the resulting soot volume fraction, the development of more accurate source terms for the  $N_C$  equation would provide important details regarding soot particle sizes.

The variety of methods proposed for calculating coal-derived soot provide various degrees of empiricism. The most developed method uses three transport equations and is capable of predicting soot particle sizes. The accuracy of these predictions appears to be good based on results from the FFB, but needs improvement to properly model regions of low soot volume fraction. Including a source term to account for oxidation of soot particles may improve the  $N_C$  model. Assuming an average soot number density does not significantly affect the ultimate soot volume fraction predictions in any of the cases considered and may be a reasonable assumption to save computational time if specific soot particle size predictions are not required. The empirical tar equation method predicted significantly different tar contours in the FPTF than the transport equation method, but predicted soot contours in the FPTF and similar gas temperature and species concentrations in the FPTF. However, the less empirical transport equation method is recommended since it can describe effects of coal type using the CPD model.

A big challenge in computational fluid dynamic codes is accurately predicting turbulence, as was apparent in the CPR and FPTF results. It is thought that the turbulence may impact soot chemistry and particle size distribution; no attempt was made here to describe these effects. Radiative scattering from soot agglomerates might influence predictions as well. More accurate radiative properties could also contribute to overall predictive capabilities. Resorting to Lagrangian statistical methods may be necessary for accurate predictions if the transport equation method is shown to be insufficient. Modeling tar ejection velocities may also be important, especially for laminar single particle cases such as the FFB. Finally, the consideration of OH as an oxidizer instead of just  $\text{O}_2$  may prove necessary for accurate predictive capabilities.

### Conclusion

A model of soot formation from coal tar was incorporated into a 3-D comprehensive coal combustion code (PCGC-3). Soot oxidation and agglomeration were also included. The model was tested versus data from a high-temperature pyrolysis reactor and two laboratory-scale coal combustors. Based on the predictions made, the following conclusions were reached.

(1) The soot model is capable of predicting soot behavior in both nonoxidizing and oxidizing environments based on predicted tar yields from the CPD coal devolatilization model.

(2) Predictions agreed well with high-temperature soot yield data from a flat flame burner, including total soot yields as a function of coal type and qualitative diameter characteristics.

(3) Computational analysis on the impact of including a soot model indicates that the gas temperatures in the flame are lowered by as much as 300 K and that local  $\text{NO}_x$  concentrations are lowered by as much as 250 ppm. The most significant differences were observed in the predictions of the fireside performance test facility, which was the largest furnace modeled. Because the impact of soot is shown to be significant in a large furnace, modeling soot in coal-fired flames is thought to be important to ensure accurate predictions.

(4) Including a soot model in comprehensive coal combustion codes is therefore expected to improve the gas temperature and  $\text{NO}_x$  concentration predictions.

(5) The average soot particle diameter seems to be calculated accurately in regions of high soot concentration using the  $N_C$  equation. Assuming an average value of  $N_C$  appears to be a reasonable alternative to save computation time without significantly affecting predictions of  $f_{v,C}$ , provided that predicted soot particle diameters are not needed.

(6) Although tar yields were adequately represented through an empirical formula in these predictions, using the more theoretical and accurate network particle devolatilization models are recommended over empirical formulas for tar predictions.

(7) The use of a soot model adds significant additional computational time; the full model may add as much as 50% to the time required to converge. Added convergence time requirements may be reduced by starting the soot model after flow parameters such as velocities and pressures have approached convergence or by initially using the quicker, more empirical models.

(8) Additional data on coal-derived soot would greatly increase the ability to perform more detailed evaluations of the model.

(9) Future related research areas involve including the effects of modeling soot oxidation by OH, improving soot optical properties, improving turbulence models, modeling tar ejection velocities, accounting for scattering of agglomerates, and accounting for the interactions between soot and turbulence.

**Acknowledgment.** This research was funded by the Advanced Combustion and Engineering Research Center at Brigham Young University. Funds for this center are received from the National Science Foundation, the State of Utah, 43 industrial participants, and the Department of Energy.

## Glossary

$A$	Arrhenius preexponential factor
$C_1$	empirical soot formation constant
$C_2$	empirical soot oxidation constant
$C_a$	collision constant
$C_{\min}$	number of carbon atoms per incipient soot particle
$c$	concentration ( $\text{mol}/\text{m}^3$ )
$d$	diameter (m)
$E$	Arrhenius activation energy ( $\text{kJ}/\text{g}\cdot\text{mol}$ )
$f$	fraction
$g$	mixture fraction variance
$k$	Boltzman's constant ( $\text{J}/\text{K}$ ) or turbulent kinetic energy ( $\text{m}^2/\text{s}^2$ )
$L_e$	mean beam path length (m)
$M$	molecular weight
$N$	number of particles
$N_C$	soot particles per unit mass (particles/kg)
$N_A$	Avogadro's number
$p$	partial pressure ( $\text{N}/\text{m}^2$ )
$R$	universal gas constant
$r_n$	reaction rate ( $\text{s}^{-1}$ )
$S$	source term ( $\text{s}^{-1}$ )
SA	total surface area ( $\text{m}^2$ )
SP	particle source term
$T$	temperature (K)
$u$	velocity (m/s)
$V$	volume ( $\text{m}^3$ )
$Y$	mass fraction

## Greek Symbols

$\beta$	local molar density ( $\text{mol}/\text{kg}$ of mixture)
$\epsilon$	emissivity or turbulent kinetic energy dissipation rate ( $\text{m}^2/\text{s}^3$ )
$\eta$	coal gas mixture fraction
$\kappa$	absorption coefficient ( $\text{m}^{-1}$ )
$\mu$	viscosity ( $\text{kg}/\text{m}\cdot\text{s}$ )
$\rho$	density ( $\text{kg}/\text{m}^3$ )
$\sigma$	Schmidt number
$\phi$	equivalence ratio

## Subscripts

AN	agglomeration of the particles per unit mass
C	carbon or soot
FC	formation of soot
FT	formation of tar
GT	gasification of tar
g	gas
$i$	the $i$ component (i.e., 1, 2, 3...)
OC	oxidation of soot
OT	oxidation of tar
T	tar
v	volumetric basis
$\lambda$	wavelength
$\perp$	perpendicular to

EF9702207